The evolution of rock friction is more sensitive to slip than elapsed time, even at near-zero slip rates.

Pathikrit Bhattacharya[a,b], **Allan M. Rubin**[b], **Terry E. Tullis**[c], **Nicholas M. Beeler**[d], **and Keishi Okazaki**[e]

[a]School of Earth and Planetary Sciences, National Institute of Science Education and Research, Bhubaneswar, India; [b]Department of Geosciences, Princeton University, Princeton, NJ, United States.; [c]Department of Earth, Environmental and Planetary Sciences, Brown University, Providence, RI, United States; [d]U.S. Geological Survey, Vancouver, WA, United States; [e]Kochi Institute for Core Sample Research, Japan Agency for Marine-Earth Science and Technology (X-star, JAMSTEC), Kochi, Japan

This manuscript was compiled on August 8, 2021

Nearly all frictional interfaces strengthen as the logarithm of time when sliding at ultra-low speeds. Observations of also logarithmic-in-time growth of interfacial contact area under such conditions has led to constitutive models which assume that this frictional strengthening results from purely time-dependent, and slip-insensitive, contact area growth. The main laboratory support for such strengthening has traditionally been derived from increases in friction during 'load-point hold' experiments, wherein a sliding interface is allowed to gradually self-relax down to sub-nanometric slip rates. In contrast, following step decreases in the shear loading rate, friction is widely reported to increase over a characteristic slip scale, independent of the magnitude of the slip-rate decrease – a signature of slip-dependent strengthening. To investigate this apparent contradiction, we subjected granite samples to a series of step decreases in shear rate of up to 3.5 orders of magnitude, and load-point holds of up to 10,000 s, such that both protocols accessed the phenomenological regime traditionally inferred to demonstrate time-dependent frictional strengthening. When modeling the resultant data, which probe interfacial slip rates ranging from 3 μms^{-1} to less than $10^{-5}\mu ms^{-1}$, we found that constitutive models where low slip-rate friction evolution mimics log-time contact area growth require parameters that differ by orders of magnitude across the different experiments. In contrast, an alternative constitutive model in which friction evolves only with interfacial slip fits most of the data well with nearly identical parameters. This leads to the surprising conclusion that frictional strengthening is dominantly slip dependent even at sub-nanometric slip rates.

Fault friction | Earthquake | Tribology

Frictional surfaces across a wide range of materials are known to strengthen at low sliding rates. In the laboratory, this strengthening is often explored through slide-hold-reslide experiments, where a sample previously driven at a constant sliding speed is perturbed by abruptly holding the external load at fixed displacement or a fixed, low, stress level (1–8). In the former protocol, which we call a load-point hold, slip along the frictional interface continues at an ever-decreasing rate as the mechanical system (testing machine plus sample) elastically unloads and the shear stress on the frictional interface decreases. For hold durations longer than a few seconds, the static friction peak observed upon resliding at the pre-hold rate has been shown to increase as the logarithm of the hold duration, across a wide range of materials including rocks (1, 4, 5, 8, 9) (Figure S1).

In providing a physical explanation for these observations of frictional strengthening, reference has often been made to the similarly logarithmic-in-time growth of interfacial contact area (in transparent polymer glasses and plastics) during periods of little to no slip (10, 11). The connection of frictional strength to contact area dates back to Bowden and Tabor (12), who imagined frictional strength of an interface (τ_f) as the product of an average velocity dependent contact strength (τ_c) (6) and the ratio of the real contact area to the total contact area (Σ_r): $\tau_f = \tau_c\Sigma_r$. Logarithmic growth of contact area is expected if contacts deform via thermally-activated creep at normal stresses close to the indentation hardness of the sample (6, 8, 13). In the Bowden and Tabor view, this contact area growth then leads to a logarithmic-in-time increase in friction measured relative to the steady-state pre- and post-hold sliding rate. One consequence of this view is that the strength increase during the hold portion of slide-hold-reslides should be predictable from the hold duration alone, and be insensitive to the small amount of interfacial slip that accumulates during the hold (4).

The largely empirical rate-state friction (RSF) equations are widely used to model such time-varying friction phenomenology in rock (4, 5, 14) and a diverse set of industrial materials (6, 15–19). However, the two most widely used versions offer opposing views of the importance of slip for friction evolution. The more commonly used Aging formulation (1, 14) predicts that frictional strengthening loses all sensitivity to slip whenever the

Significance Statement

For many decades, frictional strength increase at low slip rates has been ascribed to time-dependent contact area growth across the sliding interface. As a result, phenomenological models that correctly predict contact area growth as observed in laboratory experiments have also been widely assumed to be appropriate descriptors of frictional strength evolution. We present new experiments which impose more than 5 orders-of-magnitude slip rate reductions on granite to show that frictional strength evolution in these rocks unequivocally refutes such models. Instead, the data suggests that, even at sub-nanometric slip rates, frictional strength dominantly evolves with accrued slip. This remarkable slip-sensitivity of friction requires changes of intrinsic strength of the interface with slip that are absent from popular conceptual models of friction at the microscopic contact-scale.

P.B. and A.R. conceived the experiments; T.T. and K.O. performed the experiments; P.B. analyzed the data and wrote the manuscript; all authors provided inputs on the manuscript.

All authors declare no conflict of interest.

[2]To whom correspondence should be addressed. E-mail: path_geoalum alumni.princeton.edu

interface is subjected to a sufficiently large and rapid decrease in slip rate. In the limit of a truly stationary interface, it implies strengthening as the logarithm of time, even in the absence of slip. When viewed in conjunction with the evidence for log-time growth of contact-area across stationary interfaces, this is consistent with the Bowden and Tabor view of contact area being the primary determinant of macroscopic strength. Its more empirical alternative – the Slip formulation – instead predicts no strengthening in the absence of sliding, and retains slip-sensitivity at all slip rates (20).

Over the last three decades, phenomenological details of frictional strengthening derived from laboratory slide-hold-reslide experiments have been widely interpreted as supporting the Aging formulation view – that frictional strengthening loses sensitivity to slip under the extreme slip-rate reductions imposed during load-point holds (3–7, 21). In contrast, friction evolution in response to less extreme, but still 1–2 orders of magnitude, velocity step decreases in the laboratory demonstrates strengthening over a characteristic slip distance independent of the final slip rate, a feature consistent with the slip dependence of friction predicted by the Slip formulation (22, 23). Therefore, somewhat paradoxically, while load-point holds and large velocity-step decreases both probe the evolution of friction following large reductions in slip rate, the traditional interpretations of these two protocols seem to provide entirely contradicting versions of the processes underlying frictional strengthening.

One resolution to this paradox is to hypothesize a rate-sensitive transition from slip- to time-dependent strengthening that is hidden within the orders-of-magnitude gap in the slip rates typically probed by these two sliding protocols (24). To test this hypothesis, and to eliminate any effects of differences in samples or experimental conditions, we ran a suite of extremely large velocity step decreases (0.5 to 3.5 orders of magnitude between $3\,\mu\mathrm{ms}^{-1}$ and $0.001\,\mu\mathrm{ms}^{-1}$) and load-point holds (of durations $10 - 10^4$ s) on an initially bare granite sample, all during the same experimental run. For our experimental conditions, these extreme velocity step decreases reach slip rates as low as those accessed during hold durations of a few 100 s – durations comfortably larger than those above which time-dependent strengthening has been widely inferred (4, 5, 11). Crucially, this means that the data from either the velocity-step or slide-hold protocols are independently sufficient to test for a rate-sensitive transition from slip- to time-dependent strengthening with decreasing slip speed.

Contrary to conventional wisdom, we find that data derived from both sliding protocols support dominantly slip dependent strength evolution, even for nearly stationary surfaces (minimum estimated slip speeds $< 10^{-5}\mu$m/s). In particular, we find that the Slip equation describes most of the data quite well using nearly identical parameters, even across these many orders-of-magnitude variations in slip rate. In contrast, the Aging equation produces worse fits to the data while also requiring orders-of-magnitude variations in the inferred RSF parameters across the diverse sliding conditions. We trace these failures of the Aging equation back to one central flaw – its prediction that strength increases primarily with time and not slip following large, rapid decreases in slip rate.

Rate-State friction and probing strengthening with velocity steps and holds

Within the RSF framework (1, 5, 9, 20, 25), the friction coefficient is expressed as a function of the sliding rate (V) and the 'state variable' (θ) describing the state of the sliding surface. In its simplest form the friction equation is:

$$\mu = \frac{\tau_f}{\sigma} = \mu_* + a \ln\left(\frac{V}{V_*}\right) + b \ln\left(\frac{V_*\theta}{D_c}\right), \qquad [1]$$

where μ is the friction coefficient, τ_f is the shear stress during sliding, σ is the normal stress, and the parameters a and b determine the amplitude of the log velocity and log state dependence of friction. μ_* is the steady-state friction value at an aribtrary reference sliding speed V_*. At moderate temperatures a and b are of order 0.01 (26), much smaller than the nominal friction value μ_* of $\sim 0.6 - 0.8$. Despite being small, the rate- and state-dependence of friction is important; it determines, for example, whether surfaces slide stably at the applied loading rate ($a > b$, referred to as "velocity-strengthening"), or potentially undergo stick-slip motion ($a < b$, "velocity-weakening"). The velocity dependence is universally positive ($a > 0$) and is generally interpreted to result from a thermally-activated Arrhenius process associated with breaking chemical bonds between asperities that bridge the sliding surface (27, 28). The source of the state-dependence is poorly understood. Despite apparent similarities in the phenomenology of state evolution among many classes of solids, including rock, glass, metal, paperboard, wood, plastics and rubber (6, 8, 10, 16, 18), it is not at all obvious that the physical and chemical processes underlying this evolution are shared.

It is commonly assumed that the time derivative of the state variable, $\dot{\theta}$, can be written as functions of the current values of V and θ only, although this assumption might be somewhat restrictive (20). For decades the most widely used forms of the state evolution equations have been:

$$\text{Aging (Dieterich) Equation}: \dot{\theta} = 1 - \frac{V\theta}{D_c} \qquad [2a]$$

$$\text{Slip (Ruina) Equation}: \dot{\theta} = -\frac{V\theta}{D_c} \ln\left(\frac{V\theta}{D_c}\right) \qquad [2b]$$

where D_c is a characteristic slip scale, often associated with the size of contacting asperities on the interface (2, 20). State here has units of time.

At steady-state sliding ($\dot{\theta} = 0$), both equations yield $V\theta/D_c = 1$, or $\theta = D_c/V$, consistent with the interpretation that at steady-state θ reflects 'contact age'. For both equations, $V\theta/D_c < 1$ leads to $\dot{\theta} > 0$. We refer to this as being 'below steady state'. The increase in friction resulting from the below-steady-state increase in θ is what we mean by frictional strengthening.

The Aging and Slip formulations differ in their predictions for strengthening when $V\theta/D_c$ drops to values much smaller than 1. Given that neither equation allows for instantaneous changes in state, such 'far below steady state' regimes can be attained via sufficiently large and rapid reductions in slip rate from steady-state sliding. In response, state evolution under the Aging formulation loses all sensitivity to slip rate, as Eq. (2a) reduces to $\dot{\theta} \sim 1$. State then evolves purely as a function of time, and again invites the interpretation that state is contact age. Note that cessation of slip is not

required to satisfy $\dot{\theta} \sim 1$; it is sufficient that $\theta \ll D_c/V$. In contrast, under the Slip formulation the rate of state evolution decreases to progressively smaller values as the size of the velocity reduction increases, with no strengthening in the limit $V \to 0$. Nevertheless, in practice, due to the finite compliance of testing machines, slip speed never decays to zero. Under these circumstances, both formulations predict an approximately logarithmic-in-time increase in frictional strength during long-duration load-point holds (strictly so under the Aging formulation, as $\dot{\theta} \sim 1$) (20, 23).

Therefore, that frictional strength increases nearly logarithmically with hold duration in slide-hold-slide experiments does not by itself distinguish between evolution of friction with slip or with elapsed time.

The slip sensitivity of strengthening was explored by Beeler et al. (4) in an experiment consisting of the same sequence of holds at two very different machine stiffnesses. They showed that the rate of increase in peak friction with log hold duration was independent of the adopted stiffness, and hence independent of the very different amounts of slip that accrued during the holds. Beeler et al. interpreted these data as supporting time-dependent strengthening during holds. Together with the discovery of logarithmic-in-time contact area growth (10, 11), and the correpsondence between Aging-law-style time-dependent strengthening and contact area growth when viewed within the Bowden-Tabor picture (8, 13), the experiments of Beeler et al (4) have been cited as evidence in support of time-dependent contact-area growth leading to frictional strengthening during holds.

The strongest evidence against this viewpoint, and for the importance of slip in determining friction evolution far below steady state, comes from velocity step experiments as mentioned before. The Slip formulation, in fact, was introduced because it matches so well the results of laboratory velocity-step experiments, where friction is observed to approach its future steady-state value as roughly a decaying exponential over a characteristic slip distance (D_c), independent of the final slip speed as well as the magnitude and sign of the velocity step (20). For velocity step decreases this clearly calls into question the universality of the hypothesis that frictional strengthening far below steady state depends upon time rather than slip.

Recently, Bhattacharya et al. (23) resolved some of this conundrum by reinterpreting the slide-hold-reslide experiments of Beeler et al. Bhattacharya et al. showed that the Slip formulation can model the stiffness-independence of the healing rate inferred from the peak friction data as well as the Aging formulation, albeit over a narrower range of parameter values. Moreover, the holds preceding these peak friction values exhibit strongly stiffness-dependent stress relaxation rates which, with constant RSF parameters, cannot be captured by the Aging formulation but are well modeled by the Slip formulation. However, this does not rule out the possibility that this apparent failure of the Aging formulation has nothing to do with the prescription of state evolution, and is, instead, just an artifact of the assumption of velocity-independent RSF parameters. To explore the latter possibility, it is necessary to increase the size of the velocity-step decreases, and drop the target velocity into the range accessed by moderately long holds. This will effectively allow any rate-dependence of the RSF parameters to be detected by the rate steps alone. The Tullis rotary shear apparatus at Brown University (25, 29, 30) is uniquely suited to our purpose given that it can be servo-controlled using a resolver near the sliding interface to artificially stiffen the machine to around 30-40 times its natural stiffness (4, 23). All the experiments reported in this paper make use of this stiffened setting. Increasing the apparatus stiffness ensures that a large velocity step imposed at the load point is translated to the sample with greater fidelity. This maximizes the departure from steady state for a given velocity step decrease at the load point (31), which facilitates distinguishing slip-from time-dependence when inverting the resulting friction data.

As we will show, the dataset generated from the experiments described herein provide sufficient diagnostic power to join a growing body of work, referenced later, suggesting that (1) frictional "state" is not synonymous with contact area, and (2) slip is essential to frictional strengthening as observed in the laboratory.

Large velocity-step decreases on a stiff apparatus. The velocity steps were carried out at 25 MPa normal stress on a hollow, cylindrical sample of Westerly granite with outer and inner diameters of 54 and 44 mm (for details of the apparatus and sample see *SI Appendix* and Figures S2 and S3). The sample was initially ground flat and then roughened at a fine scale using 60 grit grinding compound. We report experimental results only after about 120 mm of slip. At these large values, the sample reached a stable, quasi-constant, steady-state velocity weakening value of $a-b \approx -0.003$ (Figure S6). Previous studies on the same apparatus under similar conditions have shown that, during the accumulation of $\sim 40-100$ mm of slip, a 70-100 μm thick layer of gouge develops on Westerly granite samples, with the total shear being accommodated in a narrow (20-30 μm wide), quasi-planar, shear zone within this gouge (29).

To estimate the slip velocity from the displacement measured by the resolver (what we term the 'load point'), we must correct for elastic deformation of the intervening material (about 5 mm of rock plus a thin layer of glue). The elastic stiffness k (expressed as friction change per differential slip distance between the surface and the load point) was determined to be 0.065 μm^{-1} (see *Materials and Methods* and *SI Appendix*, Figure S4). Assuming homogeneous shear stress and slip distribution on the sliding interface, the elastic relation between the measured shear traction on the sample (τ), the load-point displacement ($\delta_{\rm lp}$), and the surface slip (δ), is

$$\tau = k\sigma(\delta_{\rm lp} - \delta), \qquad [3]$$

Taking the time-derivative enables us to estimate the slip speed V in terms of the servo-controlled load-point velocity V_{lp} and the time-derivative of the shear load:

$$V = V_{\rm lp} - \frac{\dot{\tau}}{k\sigma}. \qquad [4]$$

Because the surface is always sliding, even at the end of the longest load-point holds ($V = 0.02 \pm 5\%$ nm s^{-1} at the end of our 10000s holds; see *SI Appendix Figure S5*), and because slip speeds and accelerations are small enough that inertia is negligible, we can relate changes in friction to changes in shear load throughout these experiments via $\Delta\mu = \Delta\tau/\sigma$.

Figure 1A shows friction data from a large number of velocity-step decreases and increases. In these tests, the sample

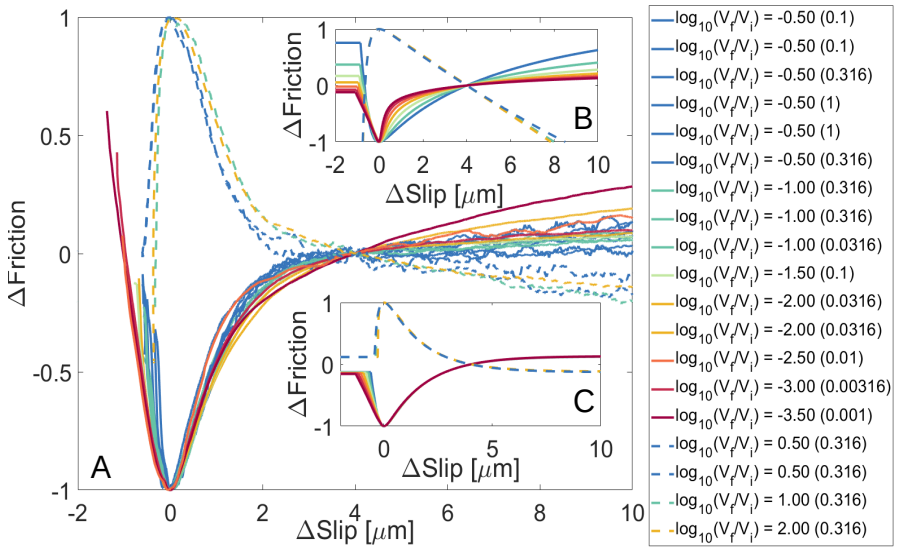

Fig. 1. (A) Large velocity-step decreases and increases on initially bare granite. Beyond 120 mm of total slip, 16 velocity-step decreases and 13 increases were carried out spanning 0.5-3.5 orders of magnitude. This plot shows 15 of these step decreases and 4 of the increases; the remainder are shown in Figure S18. The legend shows $\log_{10}(V_f/V_i)$ values coded by color; in parentheses are the final slip speeds V_f in μm/s. The slip is set to zero at the stress minimum (or maximum for the step increases). The data are smoothed over $0.2\,\mu$m for the step downs and over $0.4\,\mu$m for the step ups. The main panel shows the friction normalized by its change between 0 and $4\,\mu$m of slip. (B) and (C) show the evolution of friction for the range of step increases and decreases shown in A (colors denote step-sizes as in A) for the Aging and Slip formulations respectively. The changes in friction are measured from its value at 4μm and are normalized by the maximum amplitude of this change, as in (A). The parameters used for the Aging and Slip simulations are derived from fitting the velocity-step decreases (see *SI Appendix* and Table 1). The modeled time series is smoothed identically to the data. In (A), the friction values for the two largest step decreases begin well above zero because of the normalization scheme (the friction by 4 μm of slip remains well below its future steady state value; see Figure 2).

is initially run to steady state at a velocity $V_{lp} = V_i$, and then V_{lp} is changed to V_f over ∼0.02 s. When servo-controlling off the near-fault resolver we are able to impose sliding rates of 3 to $0.001\mu\text{ms}^{-1}$, allowing velocity jumps of up to 3.5 orders of magnitude. Previously published jumps have been limited to 2 orders of magnitude.

Each friction curve in Figure 1A has been normalized by the amplitude of its total change from its extremum to its value measured at $4\,\mu$m of slip, with slip defined as zero at the extremum. Over this initial $4\,\mu$m post-minimum slip, the plot clearly shows that frictional strength evolves over a length scale that is independent of both the step size and final slip speed V_f.

For comparison, we have plotted numerical simulations of velocity-step decreases using both the Aging formulation (Figure 1B) and the Slip formulation (Figure 1C). These simulations were run with the appropriate stiffness and a, b and D_c values derived by fitting the first 3 μm of the post-step friction evolution from a subset of the velocity steps shown in Figure 1A (see *Materials and Methods* and *SI Appendix*, Figures S6, S7 and S8).

Note, that in both the observations and the simulations, after a step decrease in V_{lp}, the stress first decreases to a minimum before increasing to its future steady-state value at $V = V_f$. In the simulations, the steep stress decay prior to the minimum is dominated by changes in the $a\ln(V/V_*)$ term in (1) (a rapid velocity drop at relatively constant state), whereas the subsequent steep stress increase is dominated by changes in the $b\ln(V_*\theta/D_c)$ term (state increases at nearly constant $V = V_f$; see *SI Appendix*, Figure S7). Therefore, across the many order-of-magnitude slip rate variations in Figure 1A, friction evolution for the first 4 μm of slip following the stress minimum represents frictional strengthening over elapsed times that vary by more than three orders of magnitude. This suggests that the collapse (for these short slip distances) of the whole suite of post-minimum velocity step data onto nearly the same curve implies the primacy of interfacial slip accumulation over time elapsed in determining this strengthening. The Slip formulation inherently captures this phenomenology, given its prediction that friction evolves to steady state over a characteristic slip scale, independent of the step size and V_f (20) (Figure 1C).

On the other hand, following a large velocity-step decrease, the Aging formulation predicts strengthening over length scales that decrease dramatically as the size of the velocity step increases (note this feature in the progression of colors subsequent to the stress minimum in Figure 1B). For velocity decreases that push the interface far below steady state ($V\theta/D_c \ll 1$), the rate of friction change with slip $d\mu/d\delta$ increases almost as rapidly with increasing velocity reduction as the velocity ratio V_i/V_f (*SI Appendix* and Figure S12). This is in clear contradiction with the data.

The velocity step data from Figure 1 are shown again as non-normalized friction versus slip in Figure 2A, with the changes in friction referenced to the pre-step steady-state level. The corresponding simulation results using the Aging and Slip formulations are shown in Figures 2D and 2E. Notably, for the experimental data the amplitude of the stress minimum $\Delta\mu_{\min}$ increases linearly with the logarithm of the size of the velocity step (inset in Figure 2A), with a slope of around -0.01. Using parameters derived from fits to the velocity-step decreases (Table 1), Slip formulation simulations also show a linear growth in $\Delta\mu_{\min}$ with log step size with a slope ~ -0.009 (Figure 2C). The data also show (Figure 2A and Figure S13 in *SI Appendix*) that the slip accumulated between the start of the velocity step and the friction minimum increases quasi-linearly with the log of the step size, again consistent with the Slip formulation simulations (Figure 2E).

The Aging formulation, on the other hand, predicts a non-linear relationship between $\Delta\mu_{\min}$ and log step size with the rate of increase in $\Delta\mu_{\min}$ decreasing systematically with larger steps (Figure 2B). In general, any increase in state (strengthening) between the onset of the velocity step and the friction minimum reduces the eventual amplitude of $\Delta\mu_{\min}$. For large velocity step decreases ($V_f/V_i \ll 1$), $V\theta/D_c \ll 1$ prior to the friction minimum. Under an Aging-style formulation this

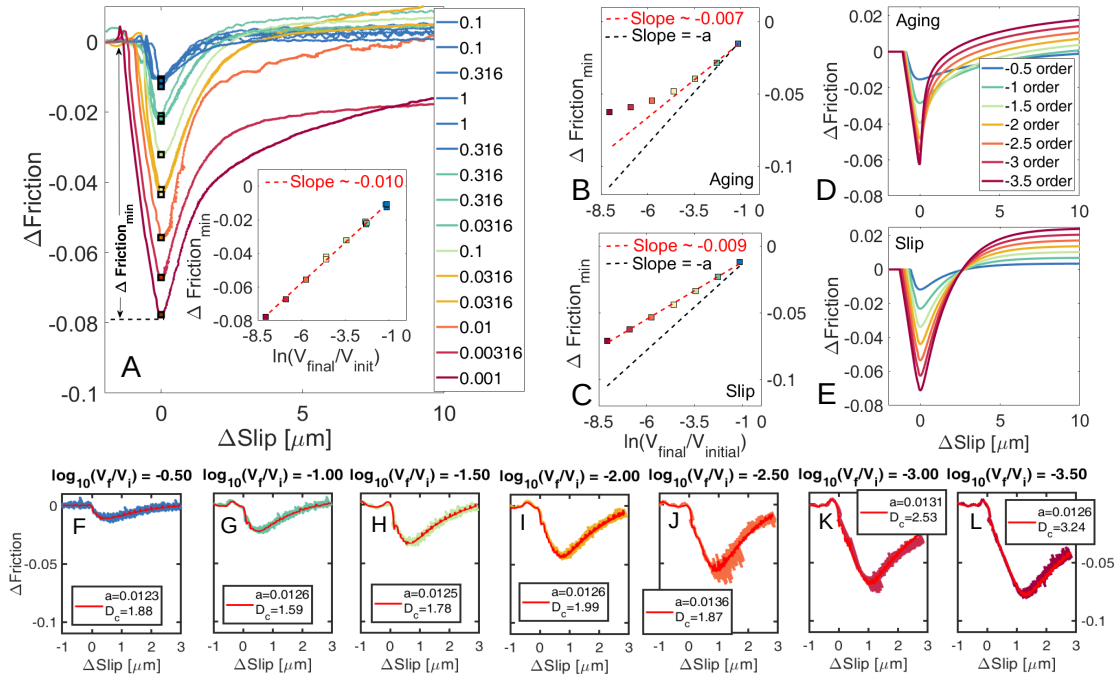

Fig. 2. (A) Same set of velocity step decreases as in Figure 1 color coded identically according to $\log_{10}(V_f/V_i)$, but plotted as non-normalized friction versus slip. The numbers in the legend show V_f in μms^{-1}. Slip is set to zero at minimum stress and shear stress is set to zero at the pre-step level. The data are smoothed as in Figure 1. Inset shows the evolution of the stress minimum ($\Delta\text{Friction}_{\min}$) with log step size. (B) Stress minima following velocity-step decreases as a function of log step size, from the (smoothed) finite stiffness simulations in Figure 1B for the Aging formulation. (C) Same as (B) but for the Slip formulation. Note that the Slip formulation predicts linear evolution of the stress minima with log step size, while the Aging formulation predicts that the stress minima deviate to significantly shallower values from the initial linear trend as step size increases, due to increased state evolution. The black dashed lines in (B) and (C) have the slope of $a = 0.0144$ for the Aging and $a = 0.013$ for the Slip formulation. The trend of the stress minima from the data in (A) is linear, as predicted by the Slip formulation. (D) and (E) show the evolution of friction for the Aging and Slip simulations of Figures 1B and 1C, respectively, but referenced to the pre-step steady value as in 2A. (F)-(L) show Slip formulation fits to one step of each size. These fits are allowed to use different a and D_c ($a - b$ for each is fixed at -0.003), and are a subset of the fits to all the step decreases in Figure S8. Note the similarity in inferred a and D_c values across the steps and the excellent fit to the data.

leads to $\dot{\theta} \sim 1$ and a much larger increase in θ prior to the friction minimum than for the Slip formulation. This leads to considerable shallowing of the curve of $\Delta\mu_{\min}$ with decreasing V_f/V_i.

Figures 2F-L show Slip formulation fits to the first 3 μm of post-step friction evolution of one each of the different step sizes in our experimental suite (all steps are fit in Figure S9). Unlike the fits used to infer the RSF parameters for the simulations in Figures 1C, 2C and 2E, the fits in Figures 2F-L allow different values of a and D_c (while fixing $a - b = -0.003$) for every velocity step shown in Figure 1A. These fits reveal that the Slip formulation requires almost no variation in a, and D_c variations of less than a factor of 2, to fit the whole suite of velocity step decreases equally well. To the extent that the larger values of D_c for the two largest velocity steps might be statistically meaningful, note that this would imply an even slower rate of fault strengthening with slip for the largest velocity reductions, whereas time-dependent strengthening requires the opposite. However, the 95% confidence intervals shown in Figure S11 seem to allow the possibility that any trends in D_c with step size are not significant.

While we have thus far focused on state evolution in response to velocity-step decreases, for completeness we point out that the velocity-step increases in Figure 1A also show systematic support for the Slip formulation. The data exhibit a quasi-characteristic length scale for stress evolution following the friction peak, independent of the sign as well as the size of the velocity step – a feature consistent with the Slip formulation (Figure 1C) (28, 32–34). The Aging formulation, in contrast, predicts linear slip weakening post-peak for velocity-step increases that push the sliding surface far above steady state ($V\theta/D_c \gg 1$) (28, 35) (see Fig. 1B). Further, since the amplitude of the friction peak increases with step size, a constant rate of weakening implies that steady state friction is attained over slip distances that also increase with step size – opposite to the trend predicted for step decreases. It is well established that such asymmetry in the frictional response between large velocity step increases and decreases is not supported by experiments (20, 22, 25, 28, 32, 36) and neither is it seen in our data.

Before concluding this section, we point out that most of our velocity step increases and decreases show a long-term evolution in stress over slip distances much larger than the D_c derived by fitting the first few microns of slip following the step. Neither the Aging nor the Slip formulation can capture this feature with a single state variable (20, 25). This is the main reason we avoid fitting more than the first 3 microns of slip following the step with our one state variable models (see *Materials and Methods*). Note that in obtaining the value $a - b = -0.003$ (supplementary Figure S6), we use the steady state values at more than 50μm of slip following our velocity steps. This value of $a - b$ probably corresponds better to a two state variable picture (25). But, on the other hand, the joint fit to the velocity steps in supplementary Figure S7,

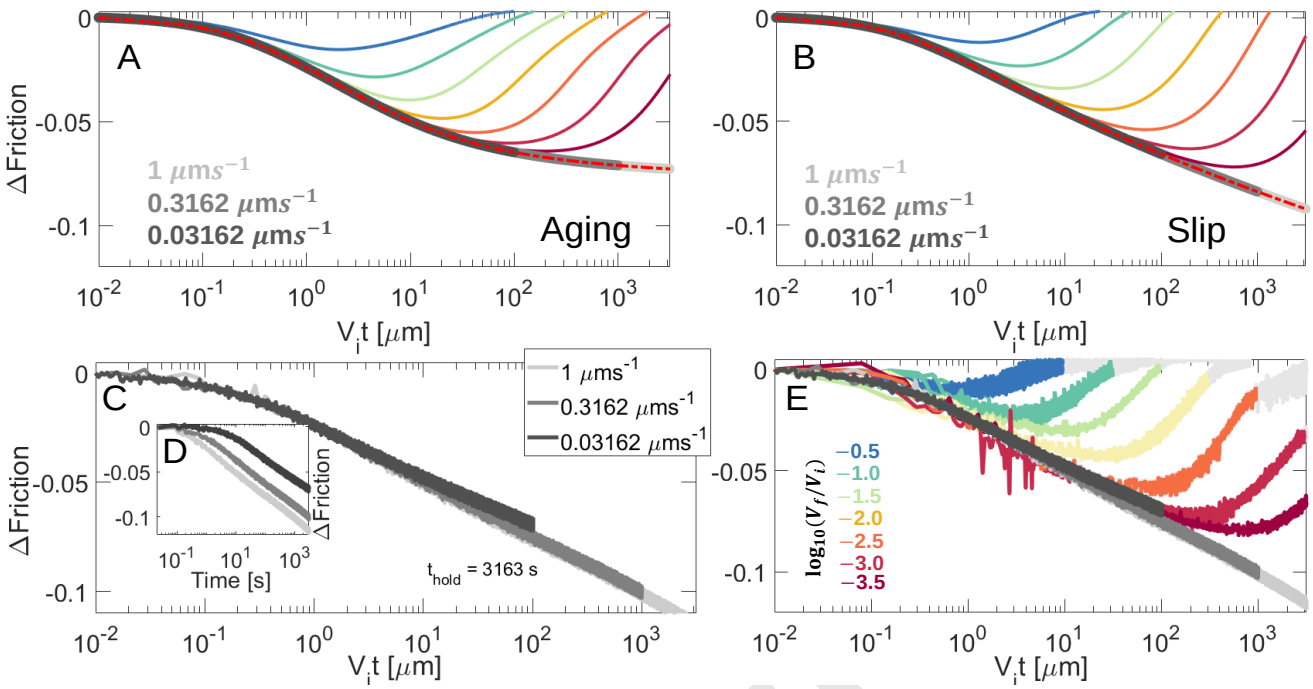

Fig. 3. Changes in friction, referenced to the prior steady-state value at slip speed V_i, for velocity-step decreases (solid colored lines) and holds (gray lines and dashed red line). Solid colored lines in (A) show the same finite stiffness simulations for the Aging formulation as in Figure 1B, now plotted vs. the logarithm of scaled time $V_i t$. The dashed red curve shows the stress relaxation trajectories of a 3000s hold with $V_i = 3\mu\text{ms}^{-1}$ and the same a, b and D_c as the velocity steps. The gray curves are for the same parameters as the red dashed curve except for the different indicated V_i. (B) is the same as (A), but for the Slip formulation with its corresponding velocity-step-derived RSF parameters. (C) shows that the friction evolution during laboratory holds of 3163 s at 3 different initial slip speeds from 0.03 to 1 μm/s collapse onto nearly the same trajectory when plotted vs. log scaled time $V_i t$. (D) shows the same data when plotted as function of time. (E) shows the same hold data and all the velocity step-decrease data of Figures (1) and (2), using the same scaling of time and color scheme as panels (A) and (B).

using the Slip formulation with a single state variable, requires $a - b = -0.003$ without any a priori constraints. Given this, and for its analytical simplicity, we have restricted ourselves to the one-state-variable picture.

In summary, the fact that the data from far below steady state – both the pre-minimum stress decrease and the post-minimum increase – are so consistent with the Slip formulation over the first few microns of slip, where (for all but the largest step) most of the post-minimum stress increase occurs, indicates that slip-dependent strengthening is responsible for most of the state evolution observed in these data. And, even when the data deviate from single-state-variable Slip formulation predictions, as do the two largest step decreases, they do so by strengthening less rapidly with slip than predicted (see also Figure S6). This is still inconsistent with time-dependent strengthening, which predicts more rapid strengthening with slip in response to larger step decreases (see *SI appendix*).

Comparing holds to the large velocity-step decreases. Our study stands apart from previous work in that it analyzes velocity step decreases and holds within a unified framework. For this reason it is useful to examine the extent to which our largest velocity step decreases and holds access similar sliding conditions. In Figure 3 we compare the stress evolution in laboratory and simulated velocity-step decreases (solid colored lines) to that in holds (gray lines). Figures 3A-B show numerical simulations comparing the shear stress relaxation during ~3000s holds from the different laboratory pre-hold driving rates we used ($V_i = 1$, 0.3 and 0.03 μms^{-1}), to the shear stress evolution following the different laboratory velocity step sizes.

In Figures 3C-E we show corresponding laboratory hold and velocity-step data with Figure 3E being the analog of Figures 3A and B.

The simulations show that most of the stress decrease between the onset of the velocity steps and the subsequent friction minimum follows the stress relaxation trajectory of the different load point holds, when the data are plotted against rescaled time $V_i t$. This scaling removes any dependence of friction evolution on V_i, within the traditional RSF framework (i.e., constant a, b and D_c with no intrinsic velocity scale; see *Materials and Methods*) (37, 38). Figure 3C applies the same scaling to data from three ~3000s holds initiated at different V_i (Figure 3D), and Figure 3E adds to this to all the velocity steps from Figure 1A. Note that the measured stress relaxations across the entire suite of holds (gray curves) also collapse to a single trajectory in Figures 3C and 3D. This is a significant result, as it provides no evidence for the hypothesis that the RSF parameters values change substantially at sliding velocities intermediate between V_i and the velocities reached by the ends of the holds (see *Materials and Methods*).

Figures 3B and E show that the velocity steps and holds share friction phenomenology down to slip rates as low as that of the largest velocity step decreases ($\sim 10^{-3}\mu\text{ms}^{-1}$). The longest holds then extend the slip rates accessed to values below $10^{-5}\mu\text{ms}^{-1}$. We show in the following section that these holds are fit well by the Slip formulation, using parameters very similar to those inferred from the velocity steps. Figure S15A shows that, for the Slip formulation, the largest velocity steps in our experiments access the same slip rates as holds of a few hundred seconds in duration irrespective of their pre-hold

sliding rates. This shows the utility of the large velocity-step decreases in our experiments – they clearly exhibit slip-dependent healing at the same sliding velocities achieved in holds long enough to clearly show logarithmic-in-time growth of both peak friction (4, 5) and contact area (10, 11).

Slide-hold experiments. Fits to our hold data (shown in Figure 4) are all constrained with $a - b = -0.003$, as determined from the steady-state friction value as a function of sliding speed (*SI Appendix* Figure S6). Holds of all durations from a particular V_i were fit jointly. The only exception are those with with $V_i = 1\mu\text{ms}^{-1}$ (Figures 4C and F), where we do not fit the two longest holds. For unknown reasons, and unlike the holds with $V_i \sim 0.3$ and $0.03\ \mu\text{ms}^{-1}$in the other panels, the longer holds with $V_i = 1\mu\text{ms}^{-1}$ do not track the trajectories of the nominally identical shorter holds over their shared duration. Figures 4A-C show fits using the Aging formulation. Although the fits up to modest values of $V_i t$ ($\lesssim 10^2$) appear not too bad, they require values of D_c orders of magnitude larger than those inferred from the velocity steps (Table 1). To rationalize this feature of the fits, we note that under an Aging formulation with $a < b$, the rate of shear stress relaxation in response to a load point hold, $d\tau/d\log(t)$, decreases with time, ultimately vanishing in the limit $V_i t \gg D_c$ (23). This is a direct implication of time-dependent strengthening ($\dot{\theta} \sim 1$ far below steady state), and can be viewed as the 'infinitely large step' limit of the pronounced shallowing of the friction minima with increasing step size already seen in Figure 2B. For $a - b = -0.003$, the Aging formulation predicts that the shear stress decay during holds begins to significantly shallow for $V_i t/D_c \gtrsim 2$, or $V_i t \gtrsim 20$ for $D_c \sim 10\mu$m (Figure 3A). The hold data, however, show nearly log-linear stress relaxation for hold durations orders of magnitude larger than this. Therefore, an Aging formulation with $a < b$ can produce good fits to these hold sequences only by requiring that D_c be not much smaller than the values of $V_i t$ accessed during these holds.

The inset in Figure 4A shows the distribution of D_c values estimated using a Monte Carlo inversion method (see *Methods and Materials*), obtained by fitting each of the three holds in the sequence individually. The inferred values of D_c increase with hold duration t_{hold}, as expected to satisfy the requirement that $V_i t_{\text{hold}}$ not be much larger than D_c. For the same reason, the inferred values of D_c increase with V_i when fitting holds of the same duration in Figures 4A–C (Table 1; the only exception to the latter statement is a second set of holds with $V_i = 0.316\ \mu\text{ms}^{-1}$ shown in Figures S16B and C).

To further evaluate the suitability of the Aging formulation to model these data, we utilize the velocity-weakening fit to the velocity steps obtained from the Aging formulation to numerically predict the stress relaxation during the longest hold in each panel (dashed orange lines in Figures 4A-C). These numerical predictions significantly underestimate the shear stress decrease observed during the longer holds. This is expected, given the velocity steps are equivalent to hold durations much shorter than the longest holds at each V_i (for relevant Aging equation predictions see Figure S14A).

In contrast to the Aging formulation, the Slip formulation fits these holds very well (Figures 4D-F) with parameters nearly identical to those inferred from the velocity steps (Table 1). For the sets of holds in Figures 4D-E, these Slip equation fits capture the observed stress relaxation across the whole range of hold durations equally well with the same set of parameters. This is formally shown in the inset of Figure 4D, where it can be seen that, in contrast to the Aging formulation, the distribution of acceptable values of D_c inferred by fitting each of the three holds in the sequence individually are statistically equivalent. For the set of holds in Figure 4F, as noted previously only the three shortest holds were fit. The D_c inferred from this set of holds is about twice as large as those in panels D and E, within the range of variation in D_c inferred when all the velocity steps are fit independently.

So, overall, and consistent with the findings of (23), the Slip equation fits to the internally consistent holds in Figures 4D-E capture the stress relaxation at the longest hold times better than the corresponding Aging equation fits. The good Slip equation fit to the shear stress data at such low slip rates (as low as 0.02 nms^{-1}; see Figure S5) implies, remarkably, that state evolution in these experiments is controlled by slip rather than elapsed time even at rates more than an order of magnitude below plate tectonic rates.

Before finishing this discussion, we point out that, unlike the holds, the corresponding reslides are not well modeled by either the Slip or the Aging formulation (Figures S17 and S18). For example, the Slip equation fits to the holds in Figures 4D-F both under-predict the static friction peaks upon resliding, and fail to capture the post-peak strength evolution (red curves in Figures S17 A-D). Therefore, neither of these widely used empirical formulations fit the entire range of laboratory data equally well.

Discussion

The main goal of this work was to determine whether the frictional strengthening of surfaces sliding at conditions far below steady state is dominantly slip-dependent or time-dependent. For both velocity step decreases and slide-hold laboratory protocols we have established that the surface strengthens (that is, state increases) primarily with slip. In doing so, we have also demonstrated that the conventional (but self-contradictory) wisdom that state evolution in response to velocity-step decreases is slip-dependent, while that in response to load-point holds is time-dependent, is incorrect. Instead, by treating holds as the limit of increasingly large velocity step decreases, we have shown that the phenomenology of frictional healing is not only slip-dependent but is well explained by the standard Slip formulation to within a few tens of percent of variation in the RSF parameters. This consistency is observed across more than 5 orders of magnitude in slip rates, from $3\mu\text{ms}^{-1}$ to $< 10^{-5}\mu\text{ms}^{-1}$.

In contrast, we have shown that any formulation in which the state contribution to friction increases as log time, analogously to the log-time contact area growth observed at low slip rates, makes the interface too strong to match the stress relaxation observed during both load-point holds and, prior to their stress minima, step velocity decreases. The Aging equation is a particular example of such a formulation.

In this context, it is worth remembering that log-time growth of contact area is not only well established in observations in transparent materials (10, 11), it also has a well-accepted theoretical basis (39). In rock, the same log-time growth of contact area has been inferred from proxy measurements of fault-normal displacement and acoustic transmissivity during load-point holds (31, 40) or from log-time compaction of granular wear material accumulated on initially bare rock in-

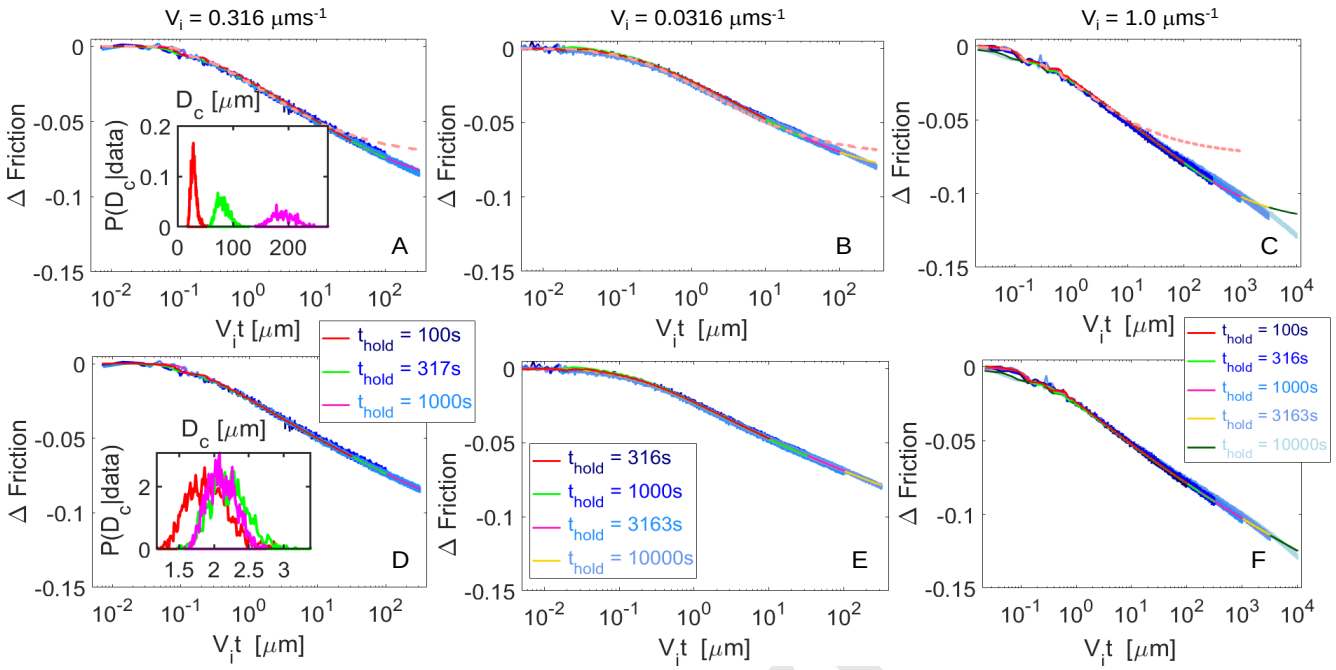

Fig. 4. Fits to the hold portions of the slide-hold-slide tests carried out during the same experimental run as the velocity steps in Figure 1. The data are represented in various shades of blue with lighter colors representing longer holds. The joint fits to all holds in each sequence are shown in the respective panels in colors other than blue. The friction change from the prior steady state is plotted as a function of scaled time $V_i t$ as in Figure 3. (A)-(C) Fits using the Aging formulation; note that these require unreasonably large values of D_c (Table 1). Dashed orange lines are predictions for the longest hold in the panel that was fit, using Aging parameters inferred from the velocity steps (see Table 1). (D)-(F) Fits to the same holds but now using the Slip formulation. The values of a and D_c required by the fits in (D) and (E) are nearly identical to those required to fit the velocity steps (Table 1 and Figure S3). The fit in (F) requires a D_c 65 % larger than that required to fit the velocity steps. The insets in (A) and (D) show the posterior distributions of D_c inferred from Monte Carlo inversions that fit the holds of different durations separately. Note that the Aging formulation requires progressively larger values of D_c for longer holds, while D_c inferred for the Slip formulation is statistically invariant across the range of hold durations. In Figures 4C and F ($V_i = 1.0$ μms^{-1}) we did not fit the two longest holds because they showed very atypical behavior – concave-down friction vs. log time curves at long hold times, and static friction peaks that decrease for hold durations longer than 10^3s (Figures 4F and S15).

Table 1. Rate-State parameters from fitting the friction data

Type	V_i	EE	TH	a	b	D_c	Fig#
Steps [a]	–	A	–	0.014	–	10.05	S4
Steps	–	A	–	0.022	0.018	0.99	S4
Holds [a]	0.032	A	10000s	0.012	–	84.85	4B
Holds [a]	0.32	A	1000s	0.013	–	103.40	4A
Holds [a]	0.32	A	3163s	0.012	–	3055.33	S16
Holds [a]	1.0	A	1000s	0.013	–	663.66	4C
Steps	–	S	–	0.013	0.016	2.07	S7
Holds [a]	0.032	S	10000s	0.014	–	1.99	4E
Holds [a]	0.32	S	1000s	0.015	–	2.10	4D
Holds [a]	0.32	S	3163s	0.014	–	4.63	S16
Holds [a]	1.0	S	1000s	0.015	–	3.43	4F

EE denotes choice of evolution equation – A for Aging, S for Slip.

TH denotes the longest hold duration fit as part of this series.

Fig# denotes the figure number for the listed fits.

V_i values in μms^{-1}, D_c in μm.

[a] denotes $a - b = -0.003$ constraint imposed on these fits.

terfaces (41). Therefore, it is quite remarkable how poorly the Aging formulation performs in reproducing friction evolution during holds, even though it mimics very well the observed phenomenology of contact area growth under similar conditions. Our results, thus, add to a growing body of evidence that the evolution of 'state' embodies more than just changes in contact area (42–45).

The bigger surprise is the extreme slip-sensitivity of friction at even sub-nanometric slip rates. Several underlying mechanisms could give rise to slip-dependent state evolution. Asperities might retain a memory of the velocity(ies) at which they formed, in which case reaching a new steady state might require swapping out the old contacts for the new, regardless of how long that takes (46). Additionally, contact area might grow during holds or normal stress increases, but that new contact area might have to undergo some strain-hardening (via slip) before reaching its steady-state strength (44). Although these ideas have been explored numerically (46, 47), no formulation developed thus far does better than the Slip formulation in describing lab friction data.

However, recent Discrete Element Method (DEM) simulations of a granular gouge layer sheared between two parallel plates, as a model for fault friction, behaved very similar to the Slip formulation with nearly constant RSF parameters during velocity-step and slide-hold protocols, consistent with laboratory experiments (48). The model gouge also underwent log-time compaction during the holds, meaning that the

DEM simulations share with lab experiments the property that although the interface normal displacements are seemingly consistent with the conventional understanding of the Aging formulation, the simulated shear stress decay follows the Slip formulation. Although these simulation results appear quite promising, the microscopic mechanisms giving rise to the macroscopically lab-like behavior remain unknown. However, granular systems are known to exhibit the same slow dynamics of other disordered systems near the 'glass transition temperature', behavior that has previously been invoked to explain non-monotonic contact area changes in PMMA at times of constant normal load (49).

It is possible, even likely, that at slip rates even lower than those accessed in our experiments, some additional process operates that involves time-dependent healing and also contributes to frictional strengthening. For example, it is known that interfaces continue to strengthen even when held truly stationary by unloading to zero shear stress (3, 6, 21, 50). It is also important to note that while the Slip formulation fits our velocity steps and holds with nearly identical parameters, it cannot fit well the peak friction upon resliding after the holds. This might indicate that the interface undergoes some additional physical change during the stress increase between the minimum at the end of the hold and the subsequent stress peak that is not captured by any existing state evolution formulation.

What also remains to be examined is the extent to which this phenomenology of rock friction extends to other materials. The clearest evidence for log-time contact area growth comes from transparent acrylic (PMMA), but PMMA samples have yet to be subjected to as exhaustive a set of sliding conditions as reported in this manuscript. This wide range of conditions has proven to be necessary to distinguish between time-dependent and slip-dependent strengthening for surfaces far below steady state. A comprehensive study of the universality of friction phenomenology among other important natural and industrial material is necessary, particularly given the diversity of materials and purposes across which RSF is used – elastomers to plastics/acrylics to metals to soft materials and micromachines (6, 15, 16, 51, 52).

Given that 'state' must in general depend upon both contact area and the quality of chemical bonding across those contacts (42, 43, 53, 54), it would be surprising if friction could be accurately described by a single state variable. It is thus remarkable that the empirical Slip formulation for state evolution does as well as it does, fitting velocity steps of both signs and load point holds with near identical parameters. This suggests that it is a good starting point for developing a state evolution formulation to better fit the reslides after holds. This is in contrast to earlier attempts at revising state evolution equations which considered time-dependent strengthening as embodied by the Aging formulation to be a desirable property of state evolution at low slip rates (24, 31). Our results, instead, show that this is the portion of the parameter space where time-dependent strengthening descriptions such as the Aging formulation are least compatible with laboratory friction data.

Materials and Methods

Estimating stiffness and $a-b$ from independent constraints. Our experiments were carried out on the Tullis rotary shear apparatus at Brown University, which was artificially stiffened using servo feedback from a near-fault transducer. To obtain an estimate of this higher stiffness, we used the initial loading curve of the reslides following a sequence of long holds carried out during the same experimental run. At the end of long holds, the block is sliding at rates orders of magnitude smaller than the pre-hold steady sliding rate V_i. Therefore, following the reslide, also at the rate V_i, there is an initial time window over which the slip rate of the block continues to satisfy $V \ll V_i$. During this initial portion of the reload, assuming quasi-static force balance between the driving shear stress and friction, we have

$$\Delta\mu = k(\delta_{lp} - \delta) = k\delta_{lp}\left(1 - \frac{\delta}{\delta_{lp}}\right) \approx k\delta_{lp}, \qquad [5]$$

where δ and δ_{lp} are surface and load point displacements since the reslide respectively, and initially $\delta/\delta_{lp} \ll 1$ for reslides following long holds. Note that k is the stiffness normalized by normal stress and $\Delta\mu$ is the change in friction. A linear fit to the $\Delta\mu$ vs. δ_{lp} plot over this initial portion following the reslide gives k as the slope (Figure S4). We use the reslides following a sequence of 3000 s and 10000 s holds carried out at three different values of V_i spanning more than an order of magnitude – 1, 0.3162 and 0.03162 μms^{-1}. For the linear fit, we chose one-seventh of the total number of points between the onset of the reslide and eventual peak strength to evaluate k. This fraction was chosen based on trial-and-error such that the spread in the estimated value of k was the least between our six chosen reslides. We found $k \sim 0.065\mu\text{m}^{-1}$ to be the mean stiffness from our fits.

For constant RSF parameters, the slope of the curve of steady-state friction vs. $\ln(V)$ is equal to $(a-b)$. In Figure S6 we show the estimation of $a-b$ from all the 0.5 to 2.0 order velocity steps in Figure 1A. The post-step steady state is chosen for all steps at 45 μm of post-minimum slip (brown stars in each panel). We did not use larger steps for $a-b$ estimation because of the prominent post-minimum transients present at 45 μm slip distance for these steps. We find that $a-b \sim -0.003$ explains the data well from the $3\mu ms^{-1}$ to $0.03\mu ms^{-1}$ slip rates covered between these steps.

Estimating a and D_c by fitting the velocity-step decreases. To constrain a and D_c, we fit either a representative size range of the velocity-step decreases (3.5-1 orders of magnitude) or all of the velocity steps in Figure 1A with the Slip equation. The forward model is simulated by equating the time derivative of $\Delta\mu$ in Eq. (5) (using the load point displacement history recorded during the experiment and $k = 0.065\mu\text{m}^{-1}$) with that in the friction law (Eq. (1)), with the Slip equation being used for state evolution (Eq. (2b)). All data are sampled uniformly at 50 Hz in these experiments. We fit the velocity step decreases in two ways – (i) parameters a, b and D_c are simultaneously and jointly inferred from all the velocity-step decreases shown in Figures S6 A-E, and (ii) parameters a and D_c are inferred independently by fitting all the velocity steps individually with the constraint that $a-b=-0.003$ (Figures S9 A-O). For the fits of type (i), we weight the misfit for each velocity step by the inverse of the total number of data samples in the fitting window to ensure that the data from all the velocity steps contribute equally to the aggregate misfit. For the inversion, we use an adaptive proposal, small-world, Markov chain Monte Carlo code. The algorithm and the general inversion procedure are described in the Supplementary materials accompanying (22). We minimize the weighted square root misfit between the modeled time series and the data at every time sample in the data. We model the evolution of friction only over the first 3 μm of slip after the onset of the velocity step. This avoids fitting secondary long term transients in the evolution of friction present in the data. For completeness, we carry out a set of Aging equation fits for all the velocity steps in Figure 1 jointly with the same a and D_c (see *SI Appendix* and Figure S8 for details). The inferred a and D_c values are reported in Table 1.

Scaling of friction response of holds and steps from different initial velocities under single-state variable RSF. Rate-state friction with constant parameter values and no intrinsic velocity scale predicts that friction evolution is independent of the pre-step or pre-hold

sliding rate V_i, when time is rescaled as $V_i t$. To show this, we begin by generalizing equation (1) to two state variables, and use V_i for the arbitrary reference velocity V_*:

$$\mu = \frac{\tau_f}{\sigma} = \mu_* + a \ln\left(\frac{V}{V_i}\right) + b_1 \ln\left(\frac{V_i\theta_1}{D_1}\right) + b_2 \ln\left(\frac{V_i\theta_2}{D_2}\right) \quad [6]$$

(extension to additional state variables is straightforward). We assume, as in equations (2), that the evolution equation for each θ_n can be expressed as a function of the dimensionless parameter $V\theta_n/D_n$:

$$\frac{d\theta_1}{dt} = F\left(\frac{V\theta_1}{D_1}\right) \; ; \quad \frac{d\theta_2}{dt} = F\left(\frac{V\theta_2}{D_2}\right). \quad [7]$$

To obtain an evolution equation for V following a velocity step or hold, dividing (3) by σ, equating this to the right hand side of (6), and taking the time derivative yields

$$\frac{dV}{dt} = V\frac{b_1}{a}\left[\frac{k}{b_1}\left(V_f - V\right) - \frac{\dot\theta_1}{\theta_1} - \frac{b_2}{b_1}\frac{\dot\theta_2}{\theta_2}\right], \quad [8]$$

where V_f is the post-step load-point velocity (zero for a hold). Next, we make (7) and (8) dimensionless by normalizing velocities by V_i and time (as well as θ_1 and θ_2) by D_1/V_i:

$$\frac{d\tilde\theta_1}{d\tilde t} = F\left(\tilde V\tilde\theta_1\right) \; ; \quad \frac{d\tilde\theta_2}{d\tilde t} = F\left(\tilde V\tilde\theta_2\frac{D_1}{D_2}\right); \quad [9]$$

$$\frac{d\tilde V}{d\tilde t} = \tilde V\frac{b_1}{a}\left[\frac{kD_1}{b_1}\left(\frac{V_f}{V_i} - \tilde V\right) - \frac{d\tilde\theta_1/d\tilde t}{\tilde\theta_1} - \frac{b_2}{b_1}\frac{d\tilde\theta_2/d\tilde t}{\tilde\theta_2}\right]; \quad [10]$$

where tildes represent dimensionless variables. Assuming steady-state sliding before the step/hold, the initial conditions on θ at the time of the step are

$$\tilde\theta_1\big|_{\tilde t=0} = 1 \; ; \quad \tilde\theta_2\big|_{\tilde t=0} = \frac{D_2}{D_1}. \quad [11]$$

Equations (9)–(11) show that, provided the RSF parameters a, b_n, and D_n are independent of sliding speed, $\tilde V(\tilde t)$ and $\tilde\theta_n(\tilde t)$ depend upon V_f/V_i (term in parentheses in (10)), but do not depend on V_i independently. Furthermore, taking the time-derivative of equation (3) and equating μ with τ/σ,

$$\frac{d\mu}{d(V_i t)} = k\left(\frac{V_f}{V_i} - \tilde V\right). \quad [12]$$

As both terms within the parentheses on the right side of (12) depend only upon V_f/V_i, again provided the RSF parameters are constant, plots of the friction change during holds should be independent of V_i when plotted vs. scaled time $V_i t$. In addition, velocity step decreases should be indistinguishable from holds as long as $V \gg V_f$. Thus, the generally clean overlap of the stress relaxation trajectories during the holds in Figure 3C is consistent with the RSF parameters being nearly constant across the > 5 orders of magnitude range of velocities accessed in these experiments.

ACKNOWLEDGMENTS. Financial support from two sources kept the Brown University lab operational during the time these experiments were conducted. Support derived from NSF grant number EAR1359596 and the Southern California Earthquake Center under grant 16026 (SCEC Contribution number 9952). SCEC is funded by NSF Cooperative agreement EAR-1600087 and USGS Cooperative Agreement G17AC00047. Support for AMR came from NSF grant number EAR1547286.

1. Dieterich JH (1972) Time-dependent friction in rocks. *J. Geophys. Res.* 77(20):3690–3697.
2. Dieterich JH (1978) Time-dependent friction and the mechanics of stick-slip. *Pure Appl. Geophys.* 116(4-5):790–806.
3. Nakatani M, Mochizuki H (1996) Effects of shear stress applied to surfaces in stationary contact on rock friction. *Geophys. Res. Lett.* 23(8):869–872.
4. Beeler N, Tullis TE, Weeks JD (1994) The roles of time and displacement in the evolution effect in rock friction. *Geophys. Res. Lett.* 21:1987–1990.
5. Marone C (1998) Laboratory derived fricition laws and their application to seismic faulting. *Annu. Rev. Earth Planet. Sci.* 26:643–696.
6. Berthoud P, Baumberger T, G'Sell C, Hiver JM (1999) Physical analysis of the state- and rate-dependent friction law: Static friction. *Phys. Rev. B* 59(22):14313–14327.
7. Karner SL, Marone C (2001) Frictional restrengthening in simulated fault gouge: Effect of shear load perturbations. *J. Geophys. Res.: Solid Earth* 106(B9):19319–19337.
8. Baumberger T, Caroli C (2006) Solid friction from stick-slip down to pinning and aging. *Adv. Phys.* 55(3-4):279–348.
9. Marone C (1998) The effect of loading rate on static friction and the rate of fault healing during the earthquake cycle. *Nature* 391:69–72.
10. Dieterich JH, Kilgore BD (1994) Direct observation of frictional contacts: New insights for state-dependent properties. *Pure Appl. Geophys.* 143:283–302.
11. Ben-David O, Rubinstein SM, Fineberg J (2010) Slip-stick and the evolution of frictional strength. *Nature* 463(7277):76–79.
12. Bowden FP, Tabor D (1964) *The Friction and Lubrication of Solids, Part 2.* (Oxford Univ. Press, New York).
13. Brechet Y, Estrin Y (1994) The effect of strain rate sensitivity on dynamic friction of metals. *Scripta Metall. Mater.* 30(11):1449 – 1454.
14. Dieterich JH (1979) Modeling of rock friction: 1. experimental results and constitutive equations. *J. Geophys. Res.* 84:2161–2168.
15. Prakash V (1998) Frictional response of sliding interfaces subjected to time varying normal pressures. *J. Tribol.* 120(1):97–102.
16. Ronsin O, Coeyrehourcq KL (2001) State, rate and temperature-dependent sliding friction of elastomers. *Proceedings of the Royal Society of London. Series A: Mathematical, Physical and Engineering Sciences* 457(2010):1277–1294.
17. Shroff SS, Ansari N, Robert Ashurst W, de Boer MP (2014) Rate-state friction in micro-electromechanical systems interfaces: Experiment and theory. *Journal of Applied Physics* 116(24):244902.
18. Heslot F, Baumberger T, Perrin B, Caroli B, Caroli C (1994) Creep, stick-slip, and dry-friction dynamics: Experiments and a heuristic model. *Phys. Rev. E* 49(6):4973–4988.
19. Carlson JM, Batista AA (1996) Constitutive relation for the friction between lubricated surfaces. *Phys. Rev. E* 53(4):4153–4165.
20. Ruina A (1983) Slip instability and state variable friction laws. *J. Geophys. Res.* 88:10,359–10,370.
21. Bureau L, Baumberger T, Caroli C (2002) Rheological aging and rejuvenation in solid friction contacts. *Eur. Phys. J. E: Soft Matter and Biological Physics* 8(3):331–337.
22. Bhattacharya P, Rubin AM, Bayart E, Savage HM, Marone C (2015) Critical evaluation of state evolution laws in rate and state friction: Fitting large velocity steps in simulated fault gouge with time-, slip-, and stress-dependent constitutive laws. *J. Geophys. Res.: Solid Earth* 120(9):6365–6385. 2015JB012437.
23. Bhattacharya P, Rubin AM, Beeler NM (2017) Does fault strengthening in laboratory rock friction experiments really depend primarily upon time and not slip? *J. Geophys. Res.: Solid Earth* 122(8):6389–6430. 2017JB013936.
24. Kato N, Tullis TE (2001) A composite rate- and state-dependent law for rock friction. *Geophys. Res. Lett.* 28(6):1103–1106.
25. Tullis TE, Weeks JD (1986) Constitutive behavior and stability of frictional sliding of granite. *Pure Appl. Geophys.* 124(3):383–414.
26. Blanpied ML, Marone CJ, Lockner DA, Byerlee JD, King DP (1998) Quantitative measure of the variation in fault rheology due to fluid-rock interactions. *J. Geophys. Res.* 103(B5):9691–9712.
27. Rice JR, Lapusta N, Ranjith K (2001) Rate and state dependent friction and the stability of sliding between elastically deformable solids. *Journal of the Mechanics and Physics of Solids* 49(9):1865 – 1898. The {JW} Hutchinson and {JR} Rice 60th Anniversary Issue.
28. Nakatani M (2001) Conceptual and physical clarification of rate and state friction: Frictional sliding as a thermally activated rheology. *J. Geophys. Res.* 106(B7):13,347–13,380.
29. Beeler NM, Tullis TE, Blanpied ML, Weeks JD (1996) Frictional behavior of large displacement experimental faults. *J. Geophys. Res.: Solid Earth* 101(B4):8697–8715.
30. Tullis TE (1997) Friction measurement apparatus in *Instruments of Science: An Historical Encyclopedia*, eds. Bud RF, Warner DJ. (Garland, New York), pp. 249–251.
31. Nagata K, Nakatani M, Yoshida S (2012) A revised rate- and state-dependent friction law obtained by constraining constitutive and evolution laws separately with laboratory data. *J. Geophys. Res.* 117:B02314.
32. Linker MF, Dieterich JH (1992) Effects of variable normal stress on rock friction: Observations and constitutive equations. *J. Geophys. Res.* 97(B4):4923–4940.
33. Rice JR (1993) Spatio-temporal complexity of slip on a fault. *J. Geophys. Res.* 98(B6):98859907.
34. Ampuero JP, Rubin AM (2008) Earthquake nucleation on rate and state faults – aging and slip laws. *J. Geophys. Res.* 113:B01302.
35. Rubin AM, Ampuero JP (2005) Earthquake nucleation on (aging) rate and state faults. *J. Geophys. Res.* 110:B11312.
36. Ruina A (1980) Ph.D. thesis (Division of Engineering, Brown University, Providence, Rhode Island).
37. Ranjith K, Rice J (1998) Stability of quasi-static slip in a single degree of freedom elastic system with rate and state dependent friction. *J. Mech. Phys. Sol.* 47(6):1207 – 1218.
38. Gu JC, Rice JR, Ruina AL, Tse ST (1984) Slip motion and stability of a single degree of freedom elastic system with rate and state dependent friction. *J. Mech. Phys. Sol.* 32(3):167 – 196.
39. Berthoud P, Baumberger T (1998) Shear stiffness of a solid–solid multicontact interface. *Proc. R. Soc. Lon. A: Mathematical, Physical and Engineering Sciences* 454(1974):1615–1634.
40. Nagata K, Kilgore BD, Beeler N, Nakatani M (2014) High-frequency imaging of elastic contrast and contact area with implications for naturally observed changes in fault properties. *J. of Geophys. Res.: Solid Earth* 119(7):5855–5875. 2014JB011014.
41. Beeler NM, Tullis TE (1997) The roles of time and displacement in velocity-dependent volumetric strain of fault zones. *J. Geophys. Res.: Solid Earth* 102(B10):22595–22609.
42. Li Q, Tullis TE, Goldsby D, Carpick RW (2011) Frictional ageing from interfacial bonding and the origins of rate and state friction. *Nature* 480(7376):233–236.
43. Thom CA, Carpick RW, Goldsby DL (2018) Constraints on the physical mechanism of frictional aging from nanoindentation. *Geophysical Research Letters* 45(24):13,306–13,311.

44. Kilgore BD, Lozos J, Beeler N, Oglesby D (2012) Laboratory observations of fault strength in response to changes in normal stress. *J. App. Mech.* 79(3):31007–1–31007–10.
45. Tullis TE, Bhattacharya P, Rubin A, Badt N, Beeler N (2020) Analysis of normal stress stepping experiments indicates that friction evolution depends on contact area quality rather than quantity in *AGU Fall Meeting*.
46. Li T, Rubin AM (2017) A microscopic model of rate and state friction evolution. *Journal of Geophysical Research: Solid Earth* 122(8):6431–6453.
47. Li T (2019) An effort to reconcile time- and slip-dependent friction evolution. *Journal of Geophysical Research: Solid Earth* 124(2):1838–1851.
48. Ferdowsi B, Rubin AM (2020) A granular physics-based view of fault friction experiments. *Journal of Geophysical Research: Solid Earth* 125(6):e2019JB019016. e2019JB019016 10.1029/2019JB019016.
49. Dillavou S, Rubinstein SM (2018) Nonmonotonic aging and memory in a frictional interface. *Phys. Rev. Lett.* 120(22):224101.
50. Karner SL, Marone C (1998) The effect of shear load on frictional healing in simulated fault gouge. *Geophysical Research Letters* 25(24):4561–4564.
51. Shroff SS, de Boer MP (2016) Full assessment of micromachine friction within the rate-state framework: Theory and validation. *Tribology Letters* 63(3):39.
52. Sahli R, et al. (2018) Evolution of real contact area under shear and the value of static friction of soft materials. *Proc. Nat. Acad. Sci.*
53. Weber B, Suhina T, Brouwer AM, Bonn D (2019) Frictional weakening of slip interfaces. *Science Advances* 5(4).
54. Tian K, Goldsby DL, Carpick RW (2018) Rate and state friction relation for nanoscale contacts: Thermally activated prandtl-tomlinson model with chemical aging. *Phys. Rev. Lett.* 120(18):186101.